

# Lithiation of Silicon Anode based on Soft X-ray Emission Spectroscopy: A Theoretical Study

Andrey Lyalin,<sup>\*,†</sup> Vladimir G. Kuznetsov,<sup>‡</sup> Akira Nakayama,<sup>¶</sup> Igor V. Abarenkov,<sup>‡</sup>  
Ilya I. Tupitsyn,<sup>‡,§</sup> Igor E. Gabis,<sup>‡</sup> Kohei Uosaki,<sup>†</sup> and Tetsuya Taketsugu<sup>||,†</sup>

<sup>†</sup>*Global Research Center for Environment and Energy Based on Nanomaterials Science (GREEN), National Institute for Materials Science (NIMS), Tsukuba 305-0044, Japan*

<sup>‡</sup>*Faculty of Physics, St Petersburg State University, Petrodvoretz, 198504 St Petersburg, Russia*

<sup>¶</sup>*Institute for Catalysis, Hokkaido University, Sapporo 001-0021, Japan*

<sup>§</sup>*Center for Advanced Studies, Peter the Great St. Petersburg Polytechnic University, Polytekhnicheskaja 29, 195251 St. Petersburg, Russia*

<sup>||</sup>*Department of Chemistry, Faculty of Science, Hokkaido University, Sapporo 060-0810, Japan*

E-mail: lyalin.andrey@nims.go.jp

January 9, 2018

## Abstract

Due to its exceptional lithium storage capacity silicon is considered as a promising candidate for anode material in lithium-ion batteries (LIBs). In the present work we demonstrate that methods of the soft X-ray emission spectroscopy (SXES) can be used as a powerful tool for the comprehensive analysis of the electronic and structural properties of lithium silicides  $\text{Li}_x\text{Si}$  forming in LIB's anode upon Si lithiation. On the

basis of density functional theory (DFT) and molecular dynamics (MD) simulations it is shown that coordination of Si atoms in  $\text{Li}_x\text{Si}$  decreases with increase in Li concentration both for the crystalline and amorphous phases. In amorphous a- $\text{Li}_x\text{Si}$  alloys Si tends to cluster forming Si-Si covalent bonds even at the high lithium concentration. It is demonstrated that the Si- $L_{2,3}$  emission bands of the crystalline and amorphous  $\text{Li}_x\text{Si}$  alloys show different spectral dependencies reflecting the process of disintegration of Si-Si network into Si clusters and chains of the different sizes upon Si lithiation. The Si- $L_{2,3}$  emission band of  $\text{Li}_x\text{Si}$  alloys become narrower and shifts towards higher energies with an increase in Li concentration. The shape of the emission band depends on the relative contribution of the X-ray radiation from the Si atoms having different coordination. This feature of the Si- $L_{2,3}$  spectra of  $\text{Li}_x\text{Si}$  alloys can be used for the detailed analysis of the Si lithiation process and LIB's anode structure identification.

## Introduction

Lithium-ion batteries (LIBs) are widely used rechargeable power sources for various electronic devices.<sup>1,2</sup> The large interest in lithium-ion batteries is stipulated by their compact size, high energy density and operating voltage, small memory and self-discharge effects.<sup>3-6</sup> However development of the highly efficient batteries progresses slowly, due to the lack of suitable electrode materials and electrolytes.<sup>1,2</sup> Lithium intercalation of the anode is one of the most important processes in lithium battery that allows it to operate. During the charge and discharge cycles lithium diffuses in and out of electrode, inducing changes in the anode morphology.<sup>7-11</sup> The structural disintegrality and cracking results in consequent fading of the capacity due to loss of electrical conductance.<sup>12-14</sup> Therefore development of the mechanically stable high-lithium-capacity anode materials based on cheap and abundant elements is an emerging task.

Silicon is one of the very promising candidates for anode materials in LIBs because it exhibits more than order of magnitude greater theoretical Li capacity (4200 mAh/g for

Li<sub>4.4</sub>Si) than conventional graphite anodes (372 mAh/g).<sup>15-17</sup> Moreover, Si is cheaper and more abundant than graphite. However, the high capacity of Si to host Li atoms results in a large volume expansion of about 400%, amorphization of Si and crumbling of the electrode.<sup>18</sup> To overcome this problem one should have detailed understanding of mechanisms of structural transformations in Si electrodes upon lithiation/delithiation processes.<sup>19</sup> Considerable efforts have been made to elucidate the origin of the degradation performance of Si anodes in LIBs with the aim to improve their stability.<sup>19-24</sup> The lithiation process of crystalline Si (c-Si) has been intensively investigated both experimentally and theoretically.<sup>11,25-35</sup>

Recent theoretical studies have been mainly focused on the modelling of lithium insertion and diffusion in c-Si,<sup>31,36,37</sup> search for the stable crystalline Li<sub>x</sub>Si phases<sup>11,25,38-41</sup> and investigation of the structural and dynamic properties of amorphous Li<sub>x</sub>Si alloys.<sup>19,28,42,43</sup> It has been demonstrated that several lithium silicide crystalline phases, LiSi,<sup>25,44</sup> Li<sub>12</sub>Si<sub>7</sub>,<sup>45,46</sup> Li<sub>7</sub>Si<sub>3</sub>,<sup>47</sup> Li<sub>13</sub>Si<sub>4</sub>,<sup>48</sup> Li<sub>15</sub>Si<sub>4</sub>,<sup>49,50</sup> Li<sub>17</sub>Si<sub>4</sub>,<sup>51</sup> and Li<sub>22</sub>Si<sub>5</sub><sup>52</sup> can be stable. These crystalline structures can be formed during high-temperature lithiation, while room temperature lithiation of c-Si often results in formation of amorphous lithium silicides a-Li<sub>x</sub>Si.<sup>53</sup> It was suggested that the lack of formation of crystalline c-Li<sub>x</sub>Si alloys at room temperature is most likely due to kinetic constraints, which means that c-Si lithiation at the room temperature is a nonequilibrium process.<sup>31</sup> After the first cycle of lithiation and delithiation c-Si becomes amorphous.<sup>29</sup> However it has been found that lithiation of c-Si is a multi-phase process, where c-Si is lithiated layer by layer.<sup>11,29,31,35,54,55</sup> Operando neutron reflectivity analysis has demonstrated that lithiation starts with the formation of a lithium enrichment zone during the first charge step.<sup>55</sup> The Li enriched area of Li<sub>x</sub>Si can be divided into a highly lithiated zone at the surface with concentration  $x \sim 2.5$  and a much less lithiated growth region with  $x \sim 0.1$  formed deep into the crystal. The thickness of the highly lithiated zone is the same for the first and second cycle, whereas the thickness of the less lithiated zone is larger for the second lithiation.<sup>55</sup> It has also been found that lithiated Si is separated from pristine c-Si by a sharp reaction front with thickness of about 1 nm, which moves into c-Si as the

reaction progresses.<sup>27,29,35</sup> It is interesting that in the case of amorphous Si recent experiments also indicate the presence of the boundary between lithiated and pristine a-Si in spite of the absence of the crystalline order in a-Si.<sup>56,57</sup> It has been suggested that as the reaction front progresses into pure a-Si, the lithiated Si has relatively constant Li concentration  $x$  in a-Li <sub>$x$</sub> Si of  $x \sim 2.5$ .<sup>56</sup> After initial lithiation to  $x \sim 2.5$ , a second step of the reaction occurs, where Li concentration increases from  $x \sim 2.5$  to  $x \sim 3.75$ .<sup>56</sup> Interestingly, several groups reported<sup>58-64</sup> that crystalline c-Li<sub>15</sub>Si<sub>4</sub> can be formed through an amorphous Li <sub>$x$</sub> Si phase, however in other works only formation of the amorphous Li <sub>$x$</sub> Si phases was observed.<sup>29,65-69</sup>

Detailed understanding of the mechanisms of such multi-phase electrochemical lithiation processes is of extraordinary importance for the development of the stable electrodes for high-performance LIBs. Such processes have been extensively studied experimentally by transmission electron microscope (TEM),<sup>27,29,56,57</sup> X-ray diffraction (XRD),<sup>53,70</sup> nuclear magnetic resonance (NMR),<sup>71,72</sup> electron energy loss spectroscopy (EELS),<sup>73</sup> neutron reflectometry (NR)<sup>55,74,75</sup> methods. However the results of experimental studies on the structural properties of electrochemically lithiated Si are still very controversial, do not provide complete understanding of the silicon lithiation process and do not give information about chemical state and electronic properties of the Li <sub>$x$</sub> Si based anode material in LIBs.

Recently, the structure, composition and electronic state of electrochemically lithiated Si(111) have been studied by methods of soft X-ray spectroscopy (SXES) combined with the X-ray diffraction with synchrotron radiation.<sup>76</sup> It has been reported that three different phases of electrochemically lithiated Si are likely formed on the Si(111) substrate: (i) a single-crystalline c-Li<sub>15</sub>Si<sub>4</sub> alloy phase, (ii) an amorphous phase of a-Li<sub>15</sub>Si<sub>4</sub> and/or a-Li<sub>13</sub>Si<sub>4</sub>, and (iii) a mixed phase of a-Li<sub>15</sub>Si<sub>4</sub> and/or a-Li<sub>13</sub>Si<sub>4</sub> (52 %) with the crystalline c-Si (48 %).<sup>76</sup> However the detailed interpretation of the experimental results has been hindered due to the absence of the theoretical data on the formation mechanisms of the Si-L<sub>2,3</sub> emission of Li <sub>$x$</sub> Si alloys.

In the present work we perform theoretical analysis of the mechanisms of formation of

the soft X-ray Si-L<sub>2,3</sub> emission of crystalline and amorphous Li<sub>x</sub>Si alloys. On the base of comparison of results of our calculations with the available experimental data we demonstrate that methods of SXES can be used as a powerful tool for the comprehensive analysis of the electronic and structural properties of crystalline and amorphous Li<sub>x</sub>Si alloys in LIBs. In particular it is shown that the energy position and shape of the Si-L<sub>2,3</sub> band provides information about disintegration of the Si network into Si clusters of the different sizes upon Si lithiation, as well as chemical structure and composition of Li<sub>x</sub>Si alloys. Therefore SXES methods can be used as a powerful tool for investigation of the lithiation process of Si and multi-phase transitions in the crystalline and amorphous structures.

## Methods

The calculations reported herein were performed using the density-functional theory (DFT) method in a plane wave (PW) basis set<sup>77</sup> as implemented in the pseudopotential-based CASTEP code.<sup>78,79</sup> We used the generalized gradient approximation (GGA) with the parametrization of Perdew-Burke-Ernzerhof (PBE)<sup>80</sup> for the exchange-correlation functional and the ultrasoft pseudopotentials (USPs)<sup>81</sup> with two projectors for each angular momentum to describe the electron-ion interactions. The cut-off energy of 280 eV has been used. In the used UCPs the  $1s^2 2s^1$  electrons of Li atom and the  $3s^2 3p^2$  electrons of Si atom have been treated as valence electrons. The structures of the crystalline Si (c-Si)<sup>82</sup> and four stable lithium silicide crystalline phases with the different concentration  $x$  of Li atoms, c-LiSi<sup>44,83</sup> ( $x=1$ ), c-Li<sub>12</sub>Si<sub>7</sub><sup>46,84</sup> ( $x=1.71$ ), c-Li<sub>13</sub>Si<sub>4</sub><sup>48</sup> ( $x=3.25$ ), and c-Li<sub>15</sub>Si<sub>4</sub><sup>49</sup> ( $x=3.75$ ) have been fully optimized and relaxed. The robust Broyden-Fletcher-Goldfarb-Shanno (BFGS) optimizer with line search has been used for optimization of cell parameters and the all-bands conjugate-gradient minimizer has been used to determine the relaxed atomic positions. The geometry optimization has been performed until the energy difference per atom, the forces on the atoms and all the stress components do not exceed the values  $1 \times 10^{-6}$  eV/atom,  $2 \times 10^{-3}$

eV/Å and  $4 \times 10^{-3}$  GPa, respectively. The convergence of the self-consistent energy was achieved with a tolerance of  $5 \times 10^{-7}$  eV/atom.

The Monkhorst-Pack<sup>85</sup> k-point meshes ( $12 \times 12 \times 12$ ), ( $5 \times 5 \times 8$ ), ( $5 \times 2 \times 3$ ), ( $6 \times 3 \times 11$ ), and ( $5 \times 5 \times 5$ ) have been used for Brillouin zone sampling of c-Si, c-LiSi, c-Li<sub>12</sub>Si<sub>7</sub>, c-Li<sub>13</sub>Si<sub>4</sub>, and c-Li<sub>15</sub>Si<sub>4</sub> structures, respectively. The used k-point meshes were chosen in such a way that the respective maximum k-point spacings  $0.0305 \text{ \AA}^{-1}$  for c-Si,  $0.0218 \text{ \AA}^{-1}$  for c-LiSi,  $0.0233 \text{ \AA}^{-1}$  for c-Li<sub>12</sub>Si<sub>7</sub>,  $0.022 \text{ \AA}^{-1}$  for c-Li<sub>13</sub>Si<sub>4</sub>, and  $0.0188 \text{ \AA}^{-1}$  for c-Li<sub>15</sub>Si<sub>4</sub>, is be approximately the same for different structures, which corresponds roughly the same accuracy of calculations. The calculated lattice constants proved to be in an excellent agreement with the corresponding experimental values, as shown in Table 1. Slight overestimation of the lattice constants with respect to the experiment is a general feature of PBE type of density functionals.<sup>86</sup>

Table 1: Optimized lattice constants of the considered crystalline Li–Si structures and the corresponding experimental values (in parentheses).

Structure	Space group	Lattice constants (Å)
Si	Cm(8)	a = 5.464 (5.431) <sup>82</sup>
LiSi	I41/a(88)	a = 9.365 (9.353), c = 5.761 (5.743) <sup>83</sup>
Li <sub>12</sub> Si <sub>7</sub>	Pnma(62)	a = 8.574 (8.596), b = 19.709 (19.775), c = 14.361 (14.319) <sup>84</sup>
Li <sub>13</sub> Si <sub>4</sub>	Pbam(55)	a = 7.958 (7.949), b = 15.158 (15.125), c = 4.451 (4.466) <sup>48</sup>
Li <sub>15</sub> Si <sub>4</sub>	I43d(220)	a = 10.654 (10.632) <sup>49</sup>

For further modeling of the amorphous structures we constructed 2x2x2 supercell for Si and 1x1x2 supercell for LiSi and Li<sub>13</sub>Si<sub>4</sub> phases in order to maintain the total number of atoms in the cell not less than 64. More specifically, the numbers of Li and Si atoms in the simulation cell are set to (Li:Si) = (0:64), (32:32), (96:56), (52:16) and (60:16) for Si, LiSi, Li<sub>12</sub>Si<sub>7</sub>, Li<sub>13</sub>Si<sub>4</sub> and Li<sub>15</sub>Si<sub>4</sub> phases, respectively. The amorphous structures of Li-Si alloys were generated by the first-principles molecular dynamics simulations via the melt-and-quench scheme, where we used the CP2K package<sup>87</sup> with the mixed Gaussian and plane-waves (GPW) approach. The PBE functional was employed as the exchange and correlation potential. The double- $\zeta$  valence plus polarization (DZVP) basis sets of the MOLOPT type<sup>88</sup>

were used to represent the atomic orbitals of the out-core electrons (3 and 4 electrons for Li and Si, respectively) in conjunction with the norm-conserving Goedecker-Teter-Hutter pseudopotentials.<sup>89,90</sup> The energy cutoff of 400 Ry was used for the auxiliary plane wave expansion of the density. Only the  $\Gamma$ -point was considered in a supercell approach. For LiSi, Li<sub>12</sub>Si<sub>7</sub>, Li<sub>13</sub>Si<sub>4</sub>, Li<sub>15</sub>Si<sub>4</sub> alloys, starting from the crystal structure, the system was first melted at 1500 K under 1 atm in the NPT ensemble for 20 ps, where the temperature and pressure was controlled by thermostats and barostats, respectively, using an isotropic cell with variable cell lengths. The time step was set to 1.0 fs. Then, the system was annealed gradually to 300 K during a run of 5 ps, followed by 5 ps of equilibration at 300 K. In the case of a-Li<sub>13</sub>Si<sub>4</sub> and a-Li<sub>15</sub>Si<sub>4</sub> four independent samples were used for further calculations to have good statistics. For modelling amorphous Si, the melting temperature was set to 2500 K with longer simulation time of 100 ps due to the high melting point of Si, and then the system was annealed to 300 K during a run of 30 ps, followed by 5 ps of equilibration at 300 K.

Neglecting the finite width of the core level, the intensity  $I(E)$  of an X-ray emission spectrum (XES) is given by the following expression:<sup>91</sup>

$$I_0(E) = E \frac{1}{N} \sum_{n,\mathbf{k}} P_n(\mathbf{k}) \delta(E - E_n(\mathbf{k}) + E_c), \quad (1)$$

where the summation over  $\mathbf{k}$  is performed over occupied states of the Brillouin zone,  $E = \hbar\omega$  is the energy of the X-ray photon,  $E_n(\mathbf{k})$  is the one-electron energy of the  $n$ th valence band,  $E_c$  is the energy of the core level,  $N$  is the number of points in the Brillouin zone, and  $P_n(\mathbf{k})$  is the probability of transition from  $n$ th valence band to the core level  $c$  per unit time.

Atomic system of units  $\hbar = e = m = 1$  are used throughout unless specified otherwise.

In the one-electron and dipole approximation, the probability  $P_n(\mathbf{k})$  of the radiative

electron transition is determined by the formula

$$P_n(\mathbf{k}) = \frac{4}{3} \left( \frac{\omega_{nc}(\mathbf{k})}{c} \right)^3 \frac{1}{2l_c + 1} \sum_{m_c, \alpha} |\langle \psi_{n\mathbf{k}} | r_\alpha | \phi_c \rangle|^2, \quad (2)$$

where  $\omega_{nc}(\mathbf{k})$  is the transition frequency,  $l_c$  is the orbital quantum number of the core vacancy and  $c$  is the speed of light,  $\psi_{n\mathbf{k}}(\mathbf{r})$  and  $\phi_c(\mathbf{r})$  are the wave functions of the  $n$ th band and the hole, respectively,  $m_c$  is the quantum number of the projection of the core hole angular momentum and index  $\alpha = -1, 0, 1$  enumerates cyclic components of the position operator  $r_\alpha$ .

In the present work the crystal wave functions  $\tilde{\psi}_{n\mathbf{k}}(\mathbf{r})$  are calculated using the plane wave basis and the ultrasoft pseudopotential scheme implemented in the CASTEP software package.<sup>78,79</sup> Such single-electron pseudo (PS) wave functions are smoothed in the atomic core regions and can not be used directly for calculating the probability of the radiative electron transition given by Eq. 2, because it is determined by the behavior of the wave functions near the nucleus. Therefore in order to calculate the dipole matrix element in Eq. 2 the all-electron (AE) orbitals have been recovered from PS wave functions using the projected augmented wave (PAW) reconstruction method<sup>92</sup> implemented in CASTEP code.<sup>78,79</sup> Different methods of recovering of AE orbitals along with the PAW method are described in details in the previous works.<sup>91,93</sup> According to the PAW approach, an AE wave function  $\psi_{n\mathbf{k}}(\mathbf{r})$  can be recovered from the corresponding PS wave function  $\tilde{\psi}_{n\mathbf{k}}(\mathbf{r})$  by a linear transformation

$$\psi_{n\mathbf{k}}(\mathbf{r}) = \tilde{\psi}_{n\mathbf{k}}(\mathbf{r}) + \sum_i (\phi_i - \tilde{\phi}_i) \langle \tilde{p}_i | \tilde{\psi}_{n\mathbf{k}}(\mathbf{r}) \rangle, \quad (3)$$

where  $\phi_i$  and  $\tilde{\phi}_i$  are AE and PS partial waves, respectively, and  $\tilde{p}_i$  are the PAW projector functions<sup>92</sup> localized within the augmentation region and forming a basis set dual to  $\tilde{\phi}_i$ , i.e.  $\langle \tilde{p}_i | \tilde{\phi}_j \rangle = \delta_{i,j}$ . Using this transformation the dipole matrix element can be written as

follows

$$\langle \psi_{n\mathbf{k}} | r_\alpha | \phi_c \rangle = \langle \tilde{\psi}_{n\mathbf{k}} | r_\alpha | \phi_c \rangle + \sum_i \left( \langle \phi_i | r_\alpha | \phi_c \rangle - \langle \tilde{\phi}_i | r_\alpha | \phi_c \rangle \right) \langle \tilde{p}_i | \tilde{\psi}_{n\mathbf{k}}(\mathbf{r}) \rangle. \quad (4)$$

To calculate the dipole matrix elements and intensity of XES we used the on-the-fly generated (OTFG) ultrasoft pseudopotentials developed by Pickard as implemented in CASTEP code.<sup>78,79</sup>

Note that the OTFG pseudopotentials were originally developed in order to account for the core hole effect in the model of supercell by generating the pseudopotential of "excited" atom with the core hole.<sup>94-96</sup> However, in semiconductors and especially in metals the core hole can be effectively screened by valence electrons, which allows to calculate XES without accounting for the core hole effect on XES. Indeed, our qualitative estimates, given in the Supporting Information, show that in the case of -Si the core hole is screened before the spontaneous X-ray emission transition occurs. In the case of lithium silicides which possess metallic properties such approximation should work even better. Therefore, in the present work we do not take into account the core hole effect on XES. In this case the generated OTFG pseudopotential of Si atom differs from the usual ultrasoft pseudopotential with two projectors for each of s- and p- channels only by addition of two gamma-projectors into local d- channel during an automated generating with the help of Materials Studio graphical interface.<sup>97</sup>

The CASTEP calculations do not take into account the spin-orbit interaction. Therefore, it is not possible to distinguish the calculated XES between  $L_2$  and  $L_3$  emission bands, which are formed as a result of the electron transitions from the valence bands to the  $2p_{1/2}$  and  $2p_{3/2}$  core hole states, respectively. Therefore, to compare correctly the calculated  $L_{2,3}$  XES with the experimental ones we have used a simple model procedure generating an approximate  $L_3$  spectrum by shifting the calculated  $L_2$  spectrum on the magnitude of the experimental value of the spin-orbit splitting (0.6 eV for the Si  $L_{2,3}$ ) and applying the intensity scaling

based on the intensity ratios 2:4 for L spectra. Finally, to mimic the experimental XES we have considered an additional broadening of the theoretical spectra caused by the apparatus function and the natural width of core levels. In the present work the natural width of the Si 2p was taken equal to 0.015 eV following the data published by Krause and Fuggle<sup>98,99</sup> and the apparatus function has been modeled by the Gauss distribution with the full width half maximum of 0.3 eV. The details of calculation of such broadening are given in the Supporting Information. It should be mentioned that in the implemented broadening procedure of the calculated XES we have neglected the Auger broadening of the valence states. It is well-known that the broadening of valence states contribute to the so-called "low energy tailing" of XES.

## Results and discussion

Optimized structures of the crystalline and amorphous phases of silicon as well as LiSi, Li<sub>12</sub>Si<sub>7</sub>, Li<sub>13</sub>Si<sub>4</sub>, and Li<sub>15</sub>Si<sub>4</sub> lithium silicides with the different concentration of Li atoms are presented in Figure 1. Crystalline silicon c-Si adopts the diamond cubic crystal structure, which presents an ordered network of tetrahedrally bonded Si atoms as shown in Figure 1a for the c-Si 2x2x2 supercell. The c-LiSi structure possesses I41/a(88) space group and contains interconnected spiral chains of Si atoms in Li matrix, with the Si-Si bond length of 2.43 Å within the chain and 2.52 Å between the chains, as shown in Figure 1c for 1x1x2 supercell. Each of the Si atoms is coordinated with two neighboring atoms in the chain and one Si atom from the nearest chain. Therefore Si atoms in c-LiSi are three-fold coordinated. Coordination of Si atoms in Li<sub>x</sub>Si alloys decreases further with an increase in lithium concentration. Thus c-Li<sub>12</sub>Si<sub>7</sub> structure (Pnma(62) space group) contains a combination of pentagonal Si rings, where Si atoms are two-fold coordinated and four atomic star-like Si clusters where the central Si atom is three-fold coordinated, as it is shown in Figure 1e. The average coordination of Si in c-Li<sub>12</sub>Si<sub>7</sub> is 1.86. The c-Li<sub>13</sub>Si<sub>4</sub> structure (Pbam(55) space group) contains Si atoms

and dimers, with the average coordination number 0.5 (Figure 1g). Finally, in the Li rich c-Li<sub>15</sub>Si<sub>4</sub> I43d(220) structure Si atoms are scattered in the Li matrix at the large distances from each other without formation of the covalent bonds (Figure 1i).

In amorphous structures the ordered Si-network disintegrates. In the a-Si structure Si atoms are still coordinated with the 4 neighboring Si atoms, while in the case of the a-LiSi structure the average Si coordination number (calculated with the cut off distance 2.6 Å) decreases to 2.59. Thus silicon atoms in amorphous a-LiSi are less coordinated than in the crystalline c-LiSi. However, in the case of the Li rich structures the Si coordination slightly increases if compared with the corresponding crystalline phases up to 2.07, 1.13 and 0.75 for a-Li<sub>12</sub>Si<sub>7</sub>, a-Li<sub>13</sub>Si<sub>4</sub> and a-Li<sub>15</sub>Si<sub>4</sub>, respectively. Figures 1f, 1h and 1j demonstrate that the a-Li<sub>12</sub>Si<sub>7</sub> structure contains fragments of linear chains, triangles and tetramers, the a-Li<sub>13</sub>Si<sub>4</sub> structure contains silicon chains, atoms and dimers, while in the a-Li<sub>15</sub>Si<sub>4</sub> structure mostly the silicon atoms, dimers and trimers are observed. As a general trend coordination of Si decreases with increase in Li concentration both for the crystalline and amorphous phases. However, even at the high Li concentration in amorphous a-Li<sub>x</sub>Si alloys Si tends to form Si-Si covalent bonds in a good agreement with the results of previous theoretical calculations.<sup>19,28</sup> It is well known that soft X-ray Si-L<sub>2,3</sub> emission is strongly affected by the local environment and hence it should be very sensitive to the coordination of Si atoms. Therefore we suggest that such spectra carry information on the structural properties of the Li<sub>x</sub>Si alloys and can be used for the comprehensive analysis of mechanisms of silicon lithiation and disintegration of Si network into clusters of different sizes with increase in Li concentration.

Figure 2 shows soft X-ray Si-L<sub>2,3</sub> emission spectra calculated for the crystalline and amorphous Si, LiSi, Li<sub>12</sub>Si<sub>7</sub>, Li<sub>13</sub>Si<sub>4</sub>, and Li<sub>15</sub>Si<sub>4</sub> structures. The Si-L<sub>2,3</sub> emission spectra of the pure Si have been intensively studied both experimentally<sup>100-103</sup> and theoretically.<sup>104</sup> Experimental L<sub>2,3</sub> spectrum of c-Si exhibits two pronounced peaks at the photon energies 89.95 eV and 92.05 eV and broad shoulder at 95.2 eV with the fast decrease in slope at 97.5 eV.<sup>100</sup> These photon energies correspond to the energies -8.70 eV, -6.60 eV, and -3.45

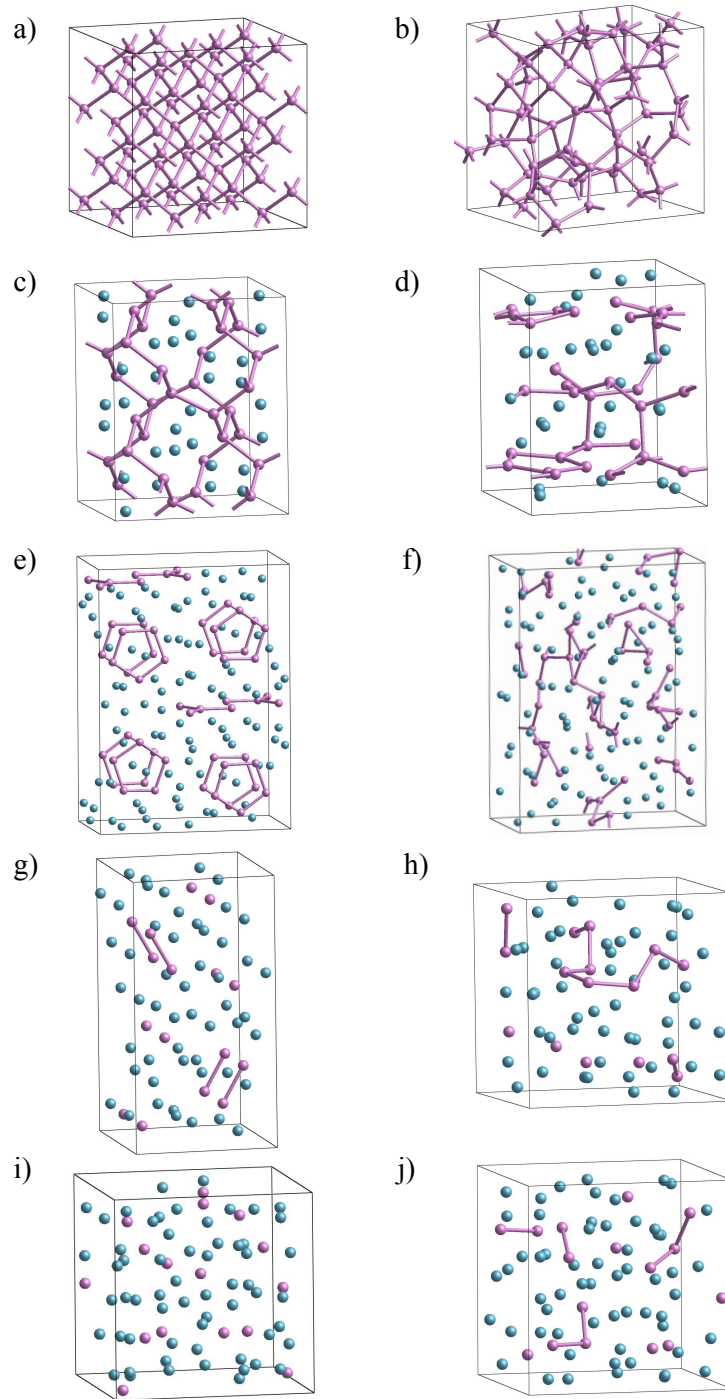


Figure 1: Optimized structures of the crystalline and amorphous phases of Si (a) and (b), and  $\text{Li}_x\text{Si}$  alloys: LiSi (c) and (d),  $\text{Li}_{12}\text{Si}_7$  (e) and (f),  $\text{Li}_{13}\text{Si}_4$  (g) and (h),  $\text{Li}_{15}\text{Si}_4$  (i) and (j). Silicon atoms are dull violet colored and lithium atoms are dull green/blue.

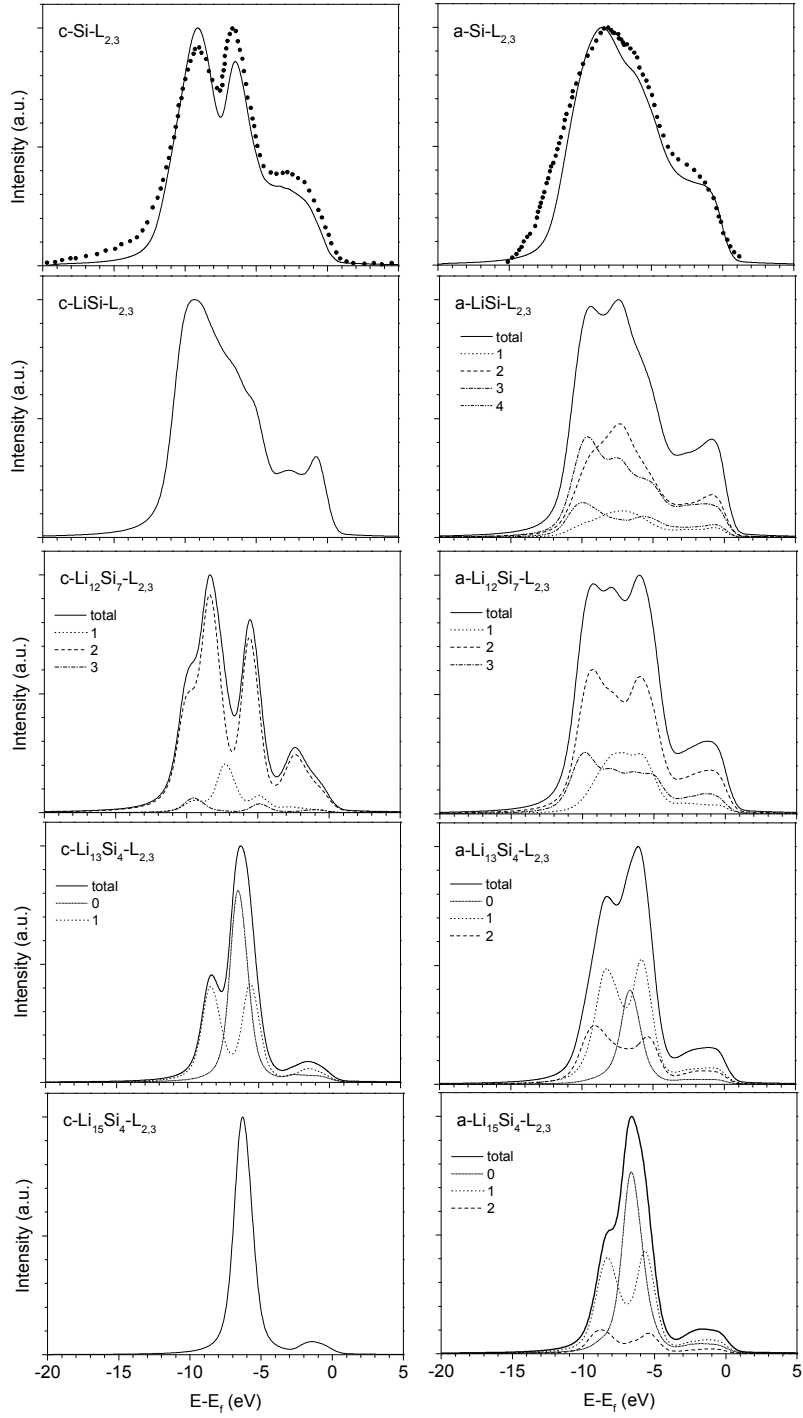


Figure 2: Soft X-ray Si-L<sub>2,3</sub> emission spectra calculated for the crystalline and amorphous Si, LiSi, Li<sub>12</sub>Si<sub>7</sub>, Li<sub>13</sub>Si<sub>4</sub>, and Li<sub>15</sub>Si<sub>4</sub> structures. Numbers 0, 1, 2, and 3 denote emission from the isolated, single, double and triple coordinated Si atoms, respectively. Black dots: experimental spectra of c-Si<sup>100</sup> and a-Si<sup>101</sup> shifted by 98.65 eV to adjust the edge of the Si-L<sub>2,3</sub> emission band to the Fermi level.

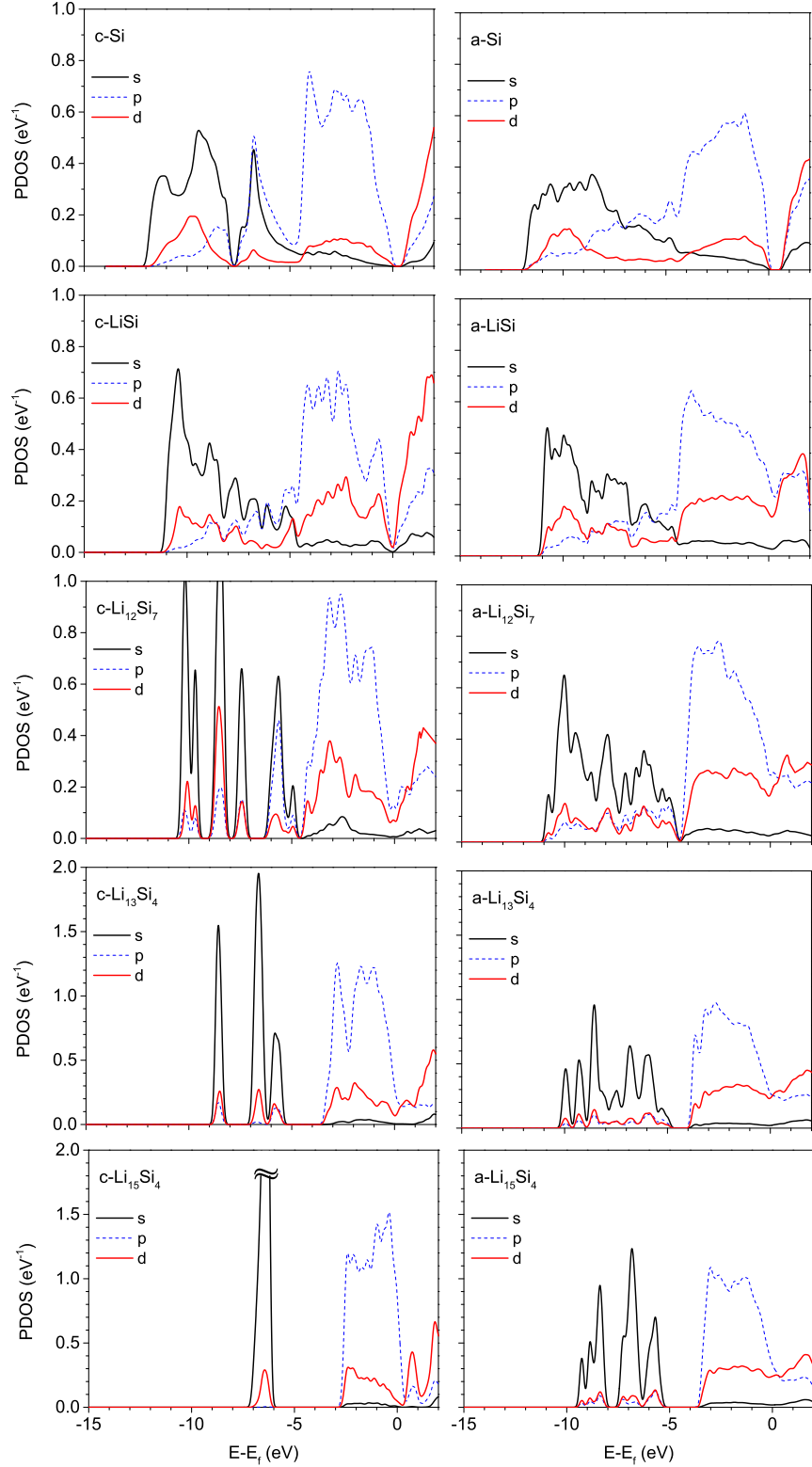


Figure 3: Partial density of electronic states (PDOS) projected on Si atoms in crystalline and amorphous Si, LiSi, Li<sub>12</sub>Si<sub>7</sub>, Li<sub>13</sub>Si<sub>4</sub>, and Li<sub>15</sub>Si<sub>4</sub> structures. Solid black, dashed blue and solid red curves represent contribution of the s, p, and d states, respectively. Gaussian broadening of half-width 0.1 eV has been used.

eV with respect to the the edge of the emission band which corresponds to the Fermi level. Figure 2 demonstrates that the Si-L<sub>2,3</sub> emission spectrum of c-Si calculated in this work reproduces very well the experimental one<sup>100</sup> represented by dots. Note that in Figure 2 the experimental spectrum is shifted by 98.65 eV to adjust the edge of the Si-L<sub>2,3</sub> emission band to the Fermi level.

We would like to emphasize that the initial state of an X-ray radiative transition is the state of an atom with a vacancy in the core shell, which can be described by the atomic orbital  $\phi_c(\mathbf{r})$  of a free atom with the quantum numbers  $n_c$ ,  $l_c$  and  $m_c$ . As a result of the one-electron radiative transition, a vacancy is formed in the valence band, which is described by the one-electron wave function  $\psi_{n\mathbf{k}}(\mathbf{r})$ . In the case of  $l_c \geq 1$ , the probability (2) of this transition can be separated into the partial contributions. Thus, in the case of the Si L<sub>2,3</sub> X-ray emission spectra (radiative electron transition to 2p vacancy of Si atom) the energy distribution of s- and d-states of the valence band mainly localized nearby the Si atom is reflected. Therefore, in order to understand formation mechanisms of the soft X-ray Si-L<sub>2,3</sub> emission bands we have calculated the partial density of electronic states (PDOS) projected on Si atoms in the considered crystalline and amorphous Li<sub>x</sub>Si alloys as shown in Figure 3. It is clearly seen that the low-energy peak in the XES of c-Si is mainly associated with the low-lying valence 3s states in the energy range of -12 eV – -8 eV, as shown in Figure 3 by black line. The second peak in the emission spectrum of c-Si corresponds to the valence states with s-p hybridization, represented by a sharp peak in PDOS with the maximum at -6.78 eV. The high energy broad peak at -3.45 eV in the Si-L<sub>2,3</sub> X-ray emission from c-Si is associated with the transitions from the 3d valence states appearing at the energies of -4 – -1 eV as a result of p-d hybridization.

In the case of amorphous silicon the Si-L<sub>2,3</sub> band exhibits a wide maximum at the photon energies 90.5 eV (-8.15 eV) with a shoulder at  $\sim$  96.5 eV (-2.15 eV)<sup>101</sup> as it is shown in Figure 2. Here numbers in parentheses correspond to the energy scale shifted by 98.65 eV to adjust the edge of the Si-L<sub>2,3</sub> emission band to the Fermi level. The main Si-L<sub>2,3</sub> emission

band of the a-Si becomes broader if compared with the one for c-Si and the second peak in the spectrum corresponding to the s-p hybridized states disappears. Indeed, PDOS of a-Si presented in Figure 3 demonstrates absence of the s-p hybridization. Therefore in the Si-L<sub>2,3</sub> spectrum of a-Si the main peak corresponds to the transitions from the s states of the valence band, while the high energy shoulder maps the d states of the valence band. The calculated Si-L<sub>2,3</sub> spectrum of a-Si excellently reproduces the experimental one, showing that the theoretical approach used in the present work is very reliable.

Lithiation considerably affects the Si-L<sub>2,3</sub> emission spectra of the crystalline and amorphous silicon. The emission band of the c-LiSi exhibits the low energy asymmetric peak with the maximum at -9.35 eV below the Fermi level, as shown in Figure 2. The right shoulder of the peak has complicated structure and drops sharply at -4 eV. The energy position of this peak is very close to the low energy peak in the Si-L<sub>2,3</sub> spectra of c-Si. It is seen from the PDOS of c-LiSi (Figure 3) that the low energy Si-L<sub>2,3</sub> emission band is mainly formed by the radiation transitions from the s valence states where a sharp low energy peak is followed by the five peaks gradually decreasing in intensity as energy increases up to -5 eV. The high energy part of the emission spectra of c-LiSi consists of a wide maximum at -2.7 eV and more sharp maximum at -0.8 eV. These two peaks originate from the d states of the valence band of c-LiSi lying in the energy range of -4 eV – 0 eV as it is seen from Figure 3. The change in the shape of the Si-L<sub>2,3</sub> emission band of c-LiSi in comparison with the pure c-Si is related to the change of the local environment of the Si atoms due to lithiation, which affects the density of the valence states of c-LiSi. As it was mentioned above Si atoms in c-LiSi are coordinated with three nearest Si atoms, while the coordination number in c-Si crystal is four. One can think that amorphization of LiSi structure would result in the smoothing of the Si-L<sub>2,3</sub> emission band shape. However, Figure 2 demonstrates that the low energy Si-L<sub>2,3</sub> band of a-LiSi has pronounced double peak structure with maxima at -9.4 eV and -7.4 eV. The similar structure also appears in the PDOS of the s states of the valence band of a-LiSi. The pronounced high energy peak in the emission spectrum at -0.9

eV is formed by the radiation transitions from the d states of the valence band. In order to understand the mechanism of formation of the double peak structure in the low energy Si-L<sub>2,3</sub> band of a-LiSi we decomposed the total emission spectrum over contributions from the Si atoms with different coordination. In Figure 2 the contributions from the groups of single-, two-, three-, and four-fold coordinated Si atoms are presented by dotted, dashed, dash-dotted and dash-double-dotted lines, respectively. As it is seen from Figure 2 the two- and three-fold coordinated Si atoms give the main contribution to the total spectrum. The spectral distribution of the emission from the two-fold coordinated Si atoms in a-LiSi has a maximum at -7.4 eV, while the main peak in the emission from the three-fold coordinated atoms is located at -9.5 eV. Therefore the double peak structure in the main Si-L<sub>2,3</sub> emission band of a-LiSi can be explained by the superposition of the photon emission from the silicon atoms with the different coordination.

The Si-L<sub>2,3</sub> emission spectrum of c-Li<sub>12</sub>Si<sub>7</sub> consists of the three well separated maxima at -8.4 eV, -5.6 eV and -2.4 eV. The high energy peak is formed by the transition from the d states of the valence band, while the two low energy peaks are formed mostly by the s states, presented in PDOS by a group of the energetically well separated sharp lines at the energies -10 eV – -5 eV. The two-fold coordinated Si atoms give dominant contribution to the whole spectrum. In the case of the amorphous a-Li<sub>12</sub>Si<sub>7</sub> lithium silicide the Si-L<sub>2,3</sub> emission spectrum shows more complicated structure with three peaks in the low energy s band at energies -9.3 eV, -8.0 eV and -6.0 eV and a broad maximum at -1.2 eV corresponding to the d band. The peaks at -9.3 eV and -6.0 eV are mostly formed by the emission from the double coordinated Si atoms with some small contribution from the triple coordinated Si atoms, while the peak in the middle of the band at -8.0 eV is formed by the emission from the single coordinated atoms, as shown in Figure 2.

As it was discussed above the c-Li<sub>13</sub>Si<sub>4</sub> structure contains an equal number of the isolated Si atoms and Si atoms forming dimers. The X-ray emission from these two groups of atoms shows different spectral dependence. The Si-L<sub>2,3</sub> emission spectrum from the isolated atoms

possesses sharp line, while the spectrum from dimers demonstrates the double peak structure, as shown in Figure 2. Therefore the total emission spectrum of  $c\text{-Li}_{13}\text{Si}_4$  shows sharp peak at -6.3 eV which corresponds mainly to the emission from the isolated Si atoms and the low energy peak at -8.3 eV corresponding to the radiation from the single coordinated Si. In the amorphous  $a\text{-Li}_{13}\text{Si}_4$  structure x-ray emission from the single and double coordinated Si atoms dominates over the one from the isolated Si. Therefore the main Si- $L_{2,3}$  emission band of  $a\text{-Li}_{13}\text{Si}_4$  becomes broader in comparison with the spectrum of the corresponding crystalline phase. The main peak in the Si- $L_{2,3}$  spectrum  $a\text{-Li}_{13}\text{Si}_4$  at -6.0 eV corresponds to the emission from the single coordinated atoms.

In the case of  $c\text{-Li}_{15}\text{Si}_4$  structure all Si atoms are separated without formation of the Si-Si covalent bonds. Therefore the Si- $L_{2,3}$  emission spectrum of  $c\text{-Li}_{15}\text{Si}_4$  possesses only one sharp intensive spectral line at -6.3 eV which corresponds to the transitions from the s states of Si and the low intensity small bump at -1.4 eV reflecting small presence of the d states in the valence band. On the other hand the emission spectra of the amorphous  $a\text{-Li}_{15}\text{Si}_4$  demonstrate low energy structure with pronounced peaks at -8.3 eV and -6.5 eV corresponding to radiation from the single coordinated and isolated Si atoms, respectively. Small contribution from the double coordinated Si atoms with a double peak structure at -8.8 eV and -5.4 eV is also noticeable. Presence of the singly and double coordinated atoms in the amorphous  $a\text{-Li}_{15}\text{Si}_4$  structure results in broadening of the the emission band. The high energy wide peak at -1.3 eV corresponds to the transitions from the d states localized in the vicinity of the single coordinated Si atoms.

Our calculations demonstrate that the Si- $L_{2,3}$  emission spectra of the crystalline and amorphous  $\text{Li}_x\text{Si}$  alloys studied in this work show very different spectral dependencies reflecting the difference in Si-Si interaction in these systems as well as the difference in disintegration of the Si-Si network into Si clusters and chains of the different sizes upon silicon lithiation. The low energy Si- $L_{2,3}$  emission bands of the  $\text{Li}_x\text{Si}$  alloys become narrower and shift towards higher energies (closer to the Fermi level) with increase in Li concentration.

Therefore the soft X-ray emission spectra of the  $\text{Li}_x\text{Si}$  alloys can be used as a powerful tool for investigation of the silicon lithiation process and transition from the crystalline to amorphous structures in LIBs.

Recently, it was demonstrated experimentally that several well separated  $\text{Li}_x\text{Si}$  phases are formed on Si(111) substrate upon electrochemical lithiation.<sup>76</sup> The above experiments have been performed with the use of methods of the soft X-ray emission spectroscopy combined with the scanning electron microscopy and the X-ray diffraction. It was suggested that the first layer formed upon electrochemical Si(111) lithiation is a single-crystalline  $\text{c-Li}_{15}\text{Si}_4$  alloy phase, while the second layer is a mixture of amorphous  $\text{a-Li}_{15}\text{Si}_4$  and/or  $\text{a-Li}_{13}\text{Si}_4$  phases.<sup>76</sup> However the detailed interpretation of the observed results was difficult due to the absence of theoretical data. In the present work we fill this gap and perform theoretical analysis of the Si- $\text{L}_{2,3}$  emission spectra of the different phases of  $\text{Li}_x\text{Si}$  alloys by comparing our results with the experimental XES reported by Aoki et al.<sup>76</sup>

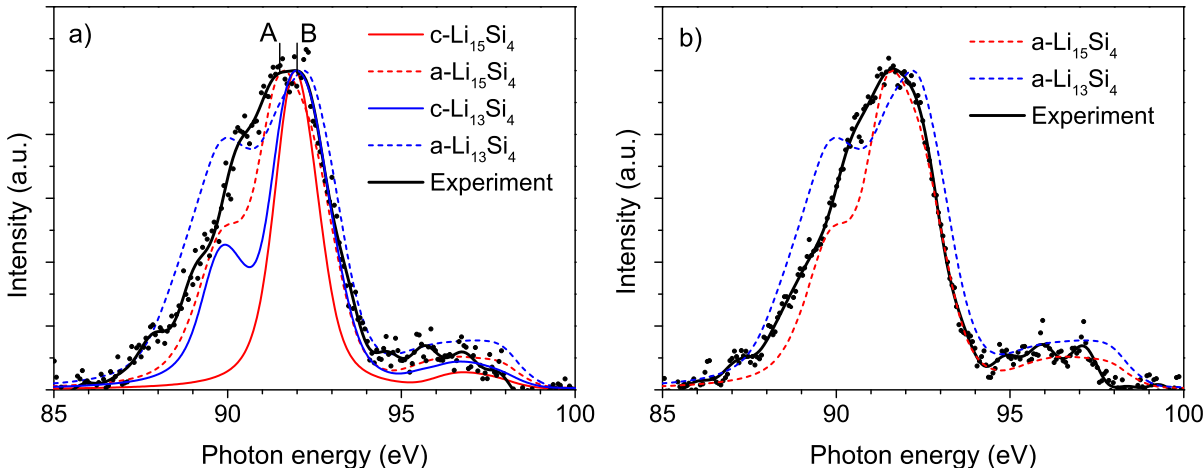


Figure 4: FFT filtered experimental Si- $\text{L}_{2,3}$  emission spectra of the first (a) and second (b) outermost layers of the electrochemically lithiated Si(111) - black lines; unfiltered experimental data - black dots.<sup>76</sup> Theoretical Si- $\text{L}_{2,3}$  emission spectra of the  $\text{c-Li}_{15}\text{Si}_4$  (red line),  $\text{a-Li}_{15}\text{Si}_4$  (red dashed line)  $\text{c-Li}_{13}\text{Si}_4$  (blue line),  $\text{a-Li}_{13}\text{Si}_4$  (blue dashed line) shifted by the experimental value<sup>76</sup> (98.24 eV) of the edge energy of the Si- $\text{L}_{2,3}$  spectra of the first and second layers.

The experimental Si- $\text{L}_{2,3}$  XES reported by Aoki et al.<sup>76</sup> for the first and second outermost layers of the electrochemically lithiated Si(111) are represented by black dots in Figures 4a

and 4b, respectively. In order to reduce an artificial noise from the spectra we perform fast Fourier transform (FFT) filtering of the experimental data. The FFT filtered spectra are shown in Figures 4a and 4b by black lines.

It was suggested by Aoki et al.<sup>76</sup> that the experimental XES of the second layer of the electrochemically lithiated Si(111) corresponds to the amorphous a-Li<sub>15</sub>Si<sub>4</sub> and/or a-Li<sub>13</sub>Si<sub>4</sub> phases. Figure 4b demonstrates that the experimental XES of the second layer is in excellent agreement with the theoretical spectrum of the a-Li<sub>15</sub>Si<sub>4</sub> phase. Note that theoretical spectra in Figure 4 are shifted by 98.24 eV which corresponds to the edge energy of Si-L<sub>2,3</sub> spectra of the first and second layers reported experimentally.<sup>76</sup> One should note, that contribution of the a-Li<sub>13</sub>Si<sub>4</sub> phase to the XES of the second layer can not be excluded completely, but lowering the concentration of lithium results in formation of the Si clusters of the larger sizes in the lithium matrix and hence broadening the Si-L<sub>2,3</sub> emission band. Figure 4b demonstrates that the calculated XES of a-Li<sub>13</sub>Si<sub>4</sub> is broader than experimental spectrum. Moreover, the energy position of the emission peak of a-Li<sub>13</sub>Si<sub>4</sub> is 0.55 eV higher in energy if compared with the one of a-Li<sub>15</sub>Si<sub>4</sub>. Therefore it is unlikely that a-Li<sub>13</sub>Si<sub>4</sub> gives noticeable contribution to the XES of the second layer observed by Aoki et al.<sup>76</sup>

The analysis of the Si-L<sub>2,3</sub> emission of the first layer is more complicated. The scanning electron microscopy image of the first layer of the electrochemically lithiated Si(111) demonstrates presence of the regular triangular pyramids with an average height of 1.0  $\mu\text{m}$  on the surface.<sup>76</sup> This observation indicates manifestation of the crystalline structure. Based on the analysis of the XRD patterns it was concluded that the first layer most likely consist of the crystalline c-Li<sub>15</sub>Si<sub>4</sub> phase.<sup>76</sup> However, comparison of the experimental XES of the first layer reported by Aoki et al.<sup>76</sup> with the results of our theoretical calculations clearly demonstrates that the X-ray emission from the first layer can not be explained by the emission from the crystalline c-Li<sub>15</sub>Si<sub>4</sub> phase only because of the considerable difference in the width and shape of the main Si-L<sub>2,3</sub> band. As it was discussed above the c-Li<sub>15</sub>Si<sub>4</sub> structure contains only isolated Si atoms, resulting in formation of the narrow spectral line in Si-L<sub>2,3</sub> emission as

shown in Figure 4a by solid red line.

One can notice that the shape of the experimental XES of the first layer in the vicinity of its maximum is flat, reflecting superposition of two peaks at  $\sim 91.5$  eV and  $\sim 92.0$  eV marked in Figure 4a as A and B, respectively. The position of the peak B ideally fits to the energy position of the spectral line of c-Li<sub>15</sub>Si<sub>4</sub> phase, while position of the peak A excellently agrees with the maximum in the XES of a-Li<sub>15</sub>Si<sub>4</sub> phase. Therefore we can conclude that XES of the first layer observed by Aoki et al.<sup>76</sup> presents superposition of the emission of the crystalline and amorphous Li<sub>15</sub>Si<sub>4</sub> phases. We should also note that energy position of the peak B fits the position of the theoretical spectra of the c-Li<sub>13</sub>Si<sub>4</sub> structure, as shown in Figure 4a, therefore we can not exclude completely contribution from the c-Li<sub>13</sub>Si<sub>4</sub> phase. Note that the shoulder on the left slope of the main band of the experimental spectrum excellently fits to the position of the low energy peak which corresponds to the emission from the single coordinated Si atoms in Si dimers or small Si chains. Such single coordinated Si atoms are absent in the c-Li<sub>15</sub>Si<sub>4</sub> phase, but manifest themselves in the a-Li<sub>15</sub>Si<sub>4</sub>, c-Li<sub>13</sub>Si<sub>4</sub> and a-Li<sub>13</sub>Si<sub>4</sub> phases. Our calculations clearly demonstrate that Si-L<sub>2,3</sub> emission bands of the crystalline and amorphous Li<sub>15</sub>Si<sub>4</sub> and Li<sub>13</sub>Si<sub>4</sub> structures are considerably different in terms of the shape and energy position and can be used for determination of the chemical structure and composition of the first layer of the electrochemically lithiated silicon. Therefore we believe that our work will stimulate intensive experimental investigation of the soft X-ray emission of the Li<sub>x</sub>Si alloys in order to resolve puzzle of the first layer.

The analysis performed above clearly demonstrates that combination of the theoretical and experimental methods of the soft X-ray emission spectroscopy can be used as a powerful tool for the comprehensive analysis of the anode materials in LIBs.

## Conclusion

In conclusion, we have shown that the methods of the soft X-ray emission spectroscopy can be used as a powerful tool for the comprehensive analysis of the electronic and structural properties of the crystalline and amorphous  $\text{Li}_x\text{Si}$  alloys forming in LIBs upon Si lithiation. DFT calculations of the crystalline and amorphous structures of Si and  $\text{LiSi}$ ,  $\text{Li}_{12}\text{Si}_7$ ,  $\text{Li}_{13}\text{Si}_4$ , and  $\text{Li}_{15}\text{Si}_4$  alloys with the different concentration of Li atoms show that the Si coordination decreases with increase in Li concentration both for the crystalline and amorphous phases, however even at the high Li concentration in amorphous  $\text{a-Li}_x\text{Si}$  alloys Si tends to cluster forming covalent Si-Si bonds. We have demonstrated that Si-L<sub>2,3</sub> emission spectra of the crystalline and amorphous  $\text{Li}_x\text{Si}$  alloys possess different spectral dependencies reflecting the difference in Si-Si interaction in these systems as well as the difference in disintegration of the Si-Si network into Si clusters and chains of the different sizes. Theoretical calculations predict that the Si-L<sub>2,3</sub> emission bands of the  $\text{Li}_x\text{Si}$  alloys become narrower and shift towards higher energies with increase in Li concentration. Comparison of the theoretical Si-L<sub>2,3</sub> emission spectra with the experimentally obtained XES from the first two layers of the electrochemically lithiated Si(111) demonstrates that XES of the top layer can be explained by the superposition of the x-ray emission from the  $\text{c-Li}_{15}\text{Si}_4$  and  $\text{a-Li}_{15}\text{Si}_4$  phases, while the second layer mostly consists of the  $\text{a-Li}_{15}\text{Si}_4$  phase. The shape and position of the Si-L<sub>2,3</sub> emission bands of  $\text{Li}_x\text{Si}$  reflect the relative contribution of the X-ray radiation from the Si atoms with different coordination which can be used for the detailed analysis of the lithiation process of Si in LIBs.

## Acknowledgement

This work was supported by the Ministry of Education, Culture, Sports, Science and Technology (MEXT) of Japan for the program on the Development of Environmental Technology using Nanotechnology; AL, AN and TT gratefully acknowledge support from the Japan

Society for the Promotion of Science (JSPS KAKENHI Grants 15K05387, 15K06563 and 16KT0047, respectively) and partial support by MEXT as "Priority Issue on Post-K computer" (Development of new fundamental technologies for high-efficiency energy creation, conversion/storage and use); IVA and VGK gratefully acknowledge support from the Russian Foundation for Basic Research (Grants 15-03-07543, 16-08-01244 and 18-03-00750). IIT acknowledges support by the Ministry of Education and Science of the Russian Federation Project No. 3.1463.2017, RFBR 15-03-07644 and RFBR 18-03-01220. The computations were performed at the Resource Center "Computer Center of SPbU", St. Petersburg, Russia; the Research Center for Computational Science, Okazaki, Japan; the Research Institute for Information Technology at Kyushu University, Japan; and the Numerical Materials Simulator, NIMS, Tsukuba, Japan. We would like to thank Prof. Toshihiro Kondo, Prof. Takahisa Ohno and Dr. Nana Aoki for fruitful discussions and Dr. Yuriko Ono for the help with visualisation of the crystal structures.

## References

- (1) Armand, M.; Tarascon, J.-M. *Nature* **2008**, *451*, 652–657.
- (2) Nitta, N.; Wu, F.; Lee, J. T.; Yushin, G. *Mater. Today* **2015**, *18*, 252 – 264.
- (3) Nazri, G.-A., Pistoia, G., Eds. *Lithium Batteries Science and Technology*; Kluwer Academic Publishers, 2004.
- (4) Tarascon, J.-M.; Armand, M. *Nature* **2001**, *414*, 359–367.
- (5) Etacheri, V.; Marom, R.; Elazari, R.; Salitra, G.; Aurbach, D. *Energy Environ. Sci.* **2011**, *4*, 3243–3262.
- (6) Sasaki, T.; Ukyo, Y.; Novák, P. *Nat Mater* **2013**, *12*, 569–575.
- (7) Huggins, R. A.; Nix, W. D. *Ionics* **2000**, *6*, 57–63.

- (8) Aifantis, K.; Hackney, S.; Dempsey, J. *J. Power Sources* **2007**, *165*, 874 – 879.
- (9) Chan, C. K.; Peng, H.; Liu, G.; McIlwrath, K.; Zhang, X. F.; Huggins, R. A.; Cui, Y. *Nat Nano* **2008**, *3*, 31–35.
- (10) Huang, J. Y.; Zhong, L.; Wang, C. M.; Sullivan, J. P.; Xu, W.; Zhang, L. Q.; Mao, S. X.; Hudak, N. S.; Liu, X. H.; Subramanian, A. et al. *Science* **2010**, *330*, 1515–1520.
- (11) Zhao, K.; Wang, W. L.; Gregoire, J.; Pharr, M.; Suo, Z.; Vlassak, J. J.; Kaxiras, E. *Nano Lett.* **2011**, *11*, 2962–2967.
- (12) Arora, P.; White, R. E.; Doyle, M. *J. Electrochem. Soc.* **1998**, *145*, 3647–3667.
- (13) Spotnitz, R. *J. Power Sources* **2003**, *113*, 72 – 80.
- (14) Sarasketa-Zabala, E.; Aguesse, F.; Villarreal, I.; Rodriguez-Martinez, L.; López, C.; Kubiak, P. *J. Phys. Chem. C* **2014**, *119*, 896–906.
- (15) Sharma, R. A.; Seefurth, R. N. *J. Electrochem. Soc.* **1976**, *123*, 1763–1768.
- (16) Boukamp, B. A.; Lesh, G. C.; Huggins, R. A. *J. Electrochem. Soc.* **1981**, *128*, 725–729.
- (17) Winter, M.; Besenhard, J. O. *Electrochim. Acta* **1999**, *45*, 31 – 50.
- (18) Obrovacz, M. N.; Christensen, L. *Electrochem. Solid-State Lett.* **2004**, *7*, A93–A96.
- (19) Chiang, H.-H.; Lu, J.-M.; Kuo, C.-L. *J. Chem. Phys.* **2016**, *144*.
- (20) Soni, S. K.; Sheldon, B. W.; Xiao, X.; Tokranov, A. *Scr. Mater.* **2011**, *64*, 307 – 310.
- (21) Xie, J.; Imanishi, N.; Zhang, T.; Hirano, A.; Takeda, Y.; Yamamoto, O. *Mater. Chem. Phys.* **2010**, *120*, 421 – 425.
- (22) Balke, N.; Jesse, S.; Kim, Y.; Adamczyk, L.; Tselev, A.; Ivanov, I. N.; Dudney, N. J.; Kalinin, S. V. *Nano Lett.* **2010**, *10*, 3420–3425.

- (23) Yoshimura, K.; Suzuki, J.; Sekine, K.; Takamura, T. *J. Power Sources* **2007**, *174*, 653 – 657, 13th International Meeting on Lithium Batteries.
- (24) Ding, N.; Xu, J.; Yao, Y.; Wegner, G.; Fang, X.; Chen, C.; Lieberwirth, I. *Solid State Ion.* **2009**, *180*, 222 – 225.
- (25) Kubota, Y.; Escano, M. C. S.; Nakanishi, H.; Kasai, H. *J. Alloys Compd.* **2008**, *458*, 151 – 157.
- (26) Zhang, Q.; Zhang, W.; Wan, W.; Cui, Y.; Wang, E. *Nano Lett.* **2010**, *10*, 3243–3249.
- (27) Chon, M. J.; Sethuraman, V. A.; McCormick, A.; Srinivasan, V.; Guduru, P. R. *Phys. Rev. Lett.* **2011**, *107*, 045503.
- (28) Kim, H.; Chou, C.-Y.; Ekerdt, J. G.; Hwang, G. S. *J. Phys. Chem. C* **2011**, *115*, 2514–2521.
- (29) Liu, X. H.; Wang, J. W.; Huang, S.; Fan, F.; Huang, X.; Liu, Y.; Krylyuk, S.; Yoo, J.; Dayeh, S. A.; Davydov, A. V. et al. *Nat Nano* **2012**, *7*, 749–756.
- (30) McDowell, M. T.; Ryu, I.; Lee, S. W.; Wang, C.; Nix, W. D.; Cui, Y. *Adv. Mater.* **2012**, *24*, 6034–6041.
- (31) Chan, M. K. Y.; Wolverton, C.; Greeley, J. P. *J. Am. Chem. Soc.* **2012**, *134*, 14362–14374, PMID: 22817384.
- (32) Pharr, M.; Zhao, K.; Wang, X.; Suo, Z.; Vlassak, J. J. *Nano Lett.* **2012**, *12*, 5039–5047.
- (33) Jung, S. C.; Choi, J. W.; Han, Y.-K. *Nano Lett.* **2012**, *12*, 5342–5347.
- (34) Morris, A. J.; Needs, R. J.; Salager, E.; Grey, C. P.; Pickard, C. J. *Phys. Rev. B* **2013**, *87*, 174108.
- (35) Cubuk, E. D.; Kaxiras, E. *Nano Lett.* **2014**, *14*, 4065–4070.

- (36) Wan, W.; Zhang, Q.; Cui, Y.; Wang, E. *J Phys Condens Matter*. **2010**, *22*, 415501.
- (37) Peng, B.; Cheng, F.; Tao, Z.; Chen, J. *J. Chem. Phys.* **2010**, *133*, 034701.
- (38) Chevrier, V. L.; Zwanziger, J. W.; Dahn, J. R. *Can. J. Phys.* **2009**, *87*, 625–632.
- (39) Chevrier, V.; Zwanziger, J.; Dahn, J. *J. Alloys Compd.* **2010**, *496*, 25 – 36.
- (40) Morris, A. J.; Grey, C. P.; Pickard, C. J. *Phys. Rev. B* **2014**, *90*, 054111.
- (41) Valencia-Jaime, I.; Sarmiento-Pérez, R.; Botti, S.; Marques, M.; Amsler, M.; Goedecker, S.; Romero, A. *J. Alloys Compd.* **2016**, *655*, 147–154, cited By 3.
- (42) Chevrier, V. L.; Dahn, J. R. *J. Electrochem. Soc.* **2010**, *157*, A392–A398.
- (43) Huang, S.; Zhu, T. *J. Power Sources* **2011**, *196*, 3664 – 3668.
- (44) Stearns, L. A.; Gryko, J.; Diefenbacher, J.; Ramachandran, G. K.; McMillan, P. F. *J. Solid State Chem.* **2003**, *173*, 251 – 258.
- (45) Nesper, R.; von Schnering, H. G.; Curda, J. *Chemische Berichte* **1986**, *119*, 3576–3590.
- (46) Leuken, H. v.; de Wijs, G. A.; van der Lugt, W.; Groot, R. A. d. *Phys. Rev. B* **1996**, *53*, 10599–10604.
- (47) Böhm, M. C.; Ramirez, R.; Nesper, R.; von Schnering, H. G. *Phys. Rev. B* **1984**, *30*, 4870–4873.
- (48) Zeilinger, M.; Fässler, T. F. *Acta Crystallographica Section E* **2013**, *69*, i81–i82.
- (49) Zeilinger, M.; Baran, V.; van Wüllen, L.; Häussermann, U.; Fässler, T. F. *Chem. Mater.* **2013**, *25*, 4113–4121.
- (50) Kubota, Y.; Escano, M. C. S.; Nakanishi, H.; Kasai, H. *J. Appl. Phys.* **2007**, *102*.

- (51) Zeilinger, M.; Benson, D.; Häussermann, U.; Fässler, T. F. *Chem. Mater.* **2013**, *25*, 1960–1967.
- (52) Nesper, R.; von Schnering, H. *J. Solid State Chem.* **1987**, *70*, 48–57, cited By 77.
- (53) Limthongkul, P.; Jang, Y.-I.; Dudney, N. J.; Chiang, Y.-M. *Acta Materialia* **2003**, *51*, 1103 – 1113.
- (54) Cubuk, E. D.; Wang, W. L.; Zhao, K.; Vlassak, J. J.; Suo, Z.; Kaxiras, E. *Nano Lett.* **2013**, *13*, 2011–2015.
- (55) Seidlhofer, B.-K.; Jerliu, B.; Trapp, M.; Hüger, E.; Risse, S.; Cubitt, R.; Schmidt, H.; Steitz, R.; Ballauff, M. *ACS Nano* **2016**, *10*, 7458–7466.
- (56) Wang, J. W.; He, Y.; Fan, F.; Liu, X. H.; Xia, S.; Liu, Y.; Harris, C. T.; Li, H.; Huang, J. Y.; Mao, S. X. et al. *Nano Lett.* **2013**, *13*, 709–715.
- (57) McDowell, M. T.; Lee, S. W.; Harris, J. T.; Korgel, B. A.; Wang, C.; Nix, W. D.; Cui, Y. *Nano Lett.* **2013**, *13*, 758–764.
- (58) Choi, Y. S.; Pharr, M.; Kang, C. S.; Son, S.-B.; Kim, S. C.; Kim, K.-B.; Roh, H.; Lee, S.-H.; Oh, K. H.; Vlassak, J. J. *J. Power Sources* **2014**, *265*, 160 – 165.
- (59) Zeng, Z.; Liu, N.; Zeng, Q.; Ding, Y.; Qu, S.; Cui, Y.; Mao, W. L. *J. Power Sources* **2013**, *242*, 732 – 735.
- (60) Son, S.-B.; Trevey, J. E.; Roh, H.; Kim, S.-H.; Kim, K.-B.; Cho, J. S.; Moon, J.-T.; DeLuca, C. M.; Maute, K. K.; Dunn, M. L. et al. *Adv. Energy Mater.* **2011**, *1*, 1199–1204.
- (61) Liu, X. H.; Zhong, L.; Huang, S.; Mao, S. X.; Zhu, T.; Huang, J. Y. *ACS Nano* **2012**, *6*, 1522–1531.

- (62) Misra, S.; Liu, N.; Nelson, J.; Hong, S. S.; Cui, Y.; Toney, M. F. *ACS Nano* **2012**, *6*, 5465–5473.
- (63) Gu, M.; Wang, Z.; Connell, J. G.; Perea, D. E.; Lauhon, L. J.; Gao, F.; Wang, C. *ACS Nano* **2013**, *7*, 6303–6309.
- (64) Liu, X. H.; Zhang, L. Q.; Zhong, L.; Liu, Y.; Zheng, H.; Wang, J. W.; Cho, J.-H.; Dayeh, S. A.; Picraux, S. T.; Sullivan, J. P. et al. *Nano Lett.* **2011**, *11*, 2251–2258.
- (65) Chan, C. K.; Ruffo, R.; Hong, S. S.; Huggins, R. A.; Cui, Y. *J. Power Sources* **2009**, *189*, 34 – 39.
- (66) Long, B. R.; Chan, M. K. Y.; Greeley, J. P.; Gewirth, A. A. *J. Phys. Chem. C* **2011**, *115*, 18916–18921.
- (67) Schroder, K. W.; Celio, H.; Webb, L. J.; Stevenson, K. J. *J. Phys. Chem. C* **2012**, *116*, 19737–19747.
- (68) Kang, C. S.; Son, S.-B.; Kim, J. W.; Kim, S. C.; Choi, Y. S.; Heo, J. Y.; Suh, S.-S.; Kim, Y.-U.; Chu, Y. Y.; Cho, J. S. et al. *J. Power Sources* **2014**, *267*, 739 – 743.
- (69) Pereira-Nabais, C.; Swiatowska, J.; Chagnes, A.; Ozanam, F.; Gohier, A.; Tran-Van, P.; Cojocaru, C.-S.; Cassir, M.; Marcus, P. *Appl. Surf. Sci.* **2013**, *266*, 5 – 16.
- (70) Li, J.; Dahn, J. R. *J. Electrochem. Soc.* **2007**, *154*, A156–A161.
- (71) Key, B.; Bhattacharyya, R.; Morcrette, M.; Seznéc, V.; Tarascon, J.-M.; Grey, C. P. *J. Am. Chem. Soc.* **2009**, *131*, 9239–9249.
- (72) Key, B.; Morcrette, M.; Tarascon, J.-M.; Grey, C. P. *J. Am. Chem. Soc.* **2011**, *133*, 503–512.
- (73) Kang, Y.-M.; Suh, S.-B.; Kim, Y.-S. *Inorg. Chem.* **2009**, *48*, 11631–11635.

- (74) DeCaluwe, S. C.; Dhar, B. M.; Huang, L.; He, Y.; Yang, K.; Owejan, J. P.; Zhao, Y.; Talin, A. A.; Dura, J. A.; Wang, H. *Phys. Chem. Chem. Phys.* **2015**, *17*, 11301–11312.
- (75) Veith, G. M.; Doucet, M.; Baldwin, J. K.; Sacci, R. L.; Fears, T. M.; Wang, Y.; Browning, J. F. *J. Phys. Chem. C* **2015**, *119*, 20339–20349.
- (76) Aoki, N.; Omachi, A.; Uosaki, K.; Kondo, T. *ChemElectroChem* **2016**, *3*, 959–965.
- (77) Payne, M. C.; Teter, M. P.; Allan, D. C.; Arias, T. A.; Joannopoulos, J. D. *Rev. Mod. Phys.* **1992**, *64*, 1045–1097.
- (78) Segall, M. D.; Lindan, P. J. D.; Probert, M. J.; Pickard, C. J.; Hasnip, P. J.; Clark, S. J.; Payne, M. C. *J. Phys.: Condens. Matter* **2002**, *14*, 2717.
- (79) Clark, S. J.; Segall, M. D.; Pickard, C. J.; Hasnip, P. J.; Probert, M. I. J.; Refson, K.; Payne, M. C. *Zeitschrift für Kristallographie - Crystalline Materials* **2005**, *220*, 567–570.
- (80) Perdew, J. P.; Burke, K.; Ernzerhof, M. *Phys. Rev. Lett.* **1996**, *77*, 3865–3868.
- (81) Vanderbilt, D. *Phys. Rev. B* **1990**, *41*, 7892–7895.
- (82) Wyckoff, R. W. G. *Crystal Structures*; John Wiley & Sons, 1963; Vol. 1.
- (83) Evers, J.; Oehlinger, G.; Sextl, G. *Eur. J. Solid State Inorg. Chem.* **1997**, *34*, 773–774.
- (84) Wu, H.; Hartman, M. R.; Udovic, T. J.; Rush, J. J.; Zhou, W.; Bowman Jr, R. C.; Vajo, J. J. *Acta Crystallographica Section B* **2007**, *63*, 63–68.
- (85) Monkhorst, H. J.; Pack, J. D. *Phys. Rev. B* **1976**, *13*, 5188.
- (86) Haas, P.; Tran, F.; Blaha, P. *Phys. Rev. B* **2009**, *79*, 085104/1–10.

- (87) VandeVondele, J.; Krack, M.; Mohamed, F.; Parrinello, M.; Chassaing, T.; Hutter, J. *Comput. Phys. Commun.* **2005**, *167*, 103 – 128.
- (88) VandeVondele, J.; Hutter, J. *J. Chem. Phys.* **2007**, *127*, 114105.
- (89) Goedecker, S.; Teter, M.; Hutter, J. *Phys. Rev. B* **1996**, *54*, 1703–1710.
- (90) Hartwigsen, C.; Goedecker, S.; Hutter, J. *Phys. Rev. B* **1998**, *58*, 3641–3662.
- (91) Ovcharenko, R. E.; Tupitsyn, I. I.; Kuznetsov, V. G.; Shulakov, A. S. *Opt. Spectrosc.* **2011**, *111*, 940–948.
- (92) Bl'ochl, P. E. *Phys. Rev. B* **1994**, *50*, 17953–17979.
- (93) Abarenkov, I. V.; Tupitsyn, I. I. *J. Chem. Phys.* **2001**, *115*, 1650–1660.
- (94) Pickard, C. J. Ab Initio Electron Loss Spectroscopy. Ph.D. thesis, Christ's College, Cambridge, 1997.
- (95) Gao, S.-P.; Pickard, C. J.; Payne, M. C.; Zhu, J.; Yuan, J. *Phys. Rev. B* **2008**, *77*, 115122.
- (96) Gao, S.-P.; Pickard, C. J.; Perlov, A.; Milman, V. *J. Phys.: Condens. Matter* **2009**, *21*, 104203.
- (97) Materials Studio 7.0. Accelrys 2013.
- (98) Krause, M. O.; Oliver, J. H. *J. Phys. Chem. Ref. Data* **1979**, *8*, 329–338.
- (99) Fuggle, J. C., Inglesfield, J. E., Eds. *Unoccupied Electronic States: Fundamentals for XANES, EELS, IPS and BIS*; Topics in Applied Physics; Springer, Berlin, Heidelberg, 1992; Vol. 69.
- (100) Wiech, G.; Zöpf, E. In *Band Structure Spectroscopy of Metals and Alloys*; Fabian, D. J., Watson, L. M., Eds.; Academic, New York, 1973.

- (101) Scimeca, T. *J. Phys. Chem. Solids* **1991**, *52*, 709–714.
- (102) Ershov, O. A.; Lukirskii, A. P. *Fiz. Tverd. Tela* **1966**, *8*, 2137–2142, [Sov. Phys. Solid State *8*, 1699-1703 (1967)].
- (103) Mashin, A. I.; Khokhlov, A. F.; Domashevskaya, É. P.; Terekhov, V. A.; Mashin, N. I. *Semiconductors* **2001**, *35*, 956–961.
- (104) Klima, J. *J. Phys. C: Solid State Phys.* **1970**, *3*, 70–85.